Kewley, S. E., Lowenberg, M. H., Neild, S. A., & Krauskopf, B. (2016). Investigation into the interaction of nose landing gear and two DOF fuselage dynamics. *Journal of Aircraft*, *53*(4), 881-891. https://doi.org/10.2514/1.C033320

Investigation into the interaction of Nose Landing Gear and two DOF Fuselage Dynamics

Sarah Kewley,* Mark Lowenberg, †

Simon Neild, ‡

University of Bristol, Bristol, BS8 1TR, United Kingdom

Bernd Krauskopf§

University of Auckland, Auckland, 1142, New Zealand

Pilots may experience vibrations in the cockpit during ground manoeuvres because of energy being transferred from the nose landing gear to the fuselage. This indicates that the fuselage dynamics could also have an effect on the dynamics of the gear. To study this interaction, a mathematical model of a nose landing gear coupled to a fuselage model with yaw and pitch degrees of freedom is developed. Results obtained by bifurcation analysis show the nature of the interaction between the two systems; in particular the two-DOF fuselage does affect the onset and subsequent severity of nose landing gear shimmy.

I. Introduction

When designing an aircraft, analysis of how it behaves on the ground must be considered. The landing gear are especially complex as they must be lightweight mechanisms that can be stowed when in flight, but are also required to withstand large loads during landing and when on the ground. One of the main issues

*PhD Student, Department of Aerospace Engineering

†Professor in Flight Dynamics, Department of Aerospace Engineering

‡Professor of Dynamics and Control, Department of Mechanical Engineering

§Professor of Applied Mathematics, Department of Mathematics, Faculty of Science

during ground manoeuvres, be it, take-off, landing or taxiing, is the phenomenon of shimmy oscillations. Shimmy is a well studied problem in engineering and can occur in any ground vehicle with a rolling wheel. It is categorised as a self-induced oscillation and was first properly understood in cars by Broulhiet[1] in the 1920s. He found that the tyre behaviour in a rolling system is fundamental to shimmy and introduced the concept of sideslip. Fromm[2] recognised the similarities of the vibrations of cars and aircraft and, while studying the effect of sideslip, found that the lateral forces acting on the wheel are coupled to the shimmy dynamics.

Due to the influence of the tyre on shimmy dynamics, many tyre models have been presented. Probably the most well known is the stretched-string model by Dietrich and Von Schlippe,[3] who considered the tyre to be an elastic string stretched around the outer edge of the wheel, which deforms via a lateral displacement. They modelled this as a straight line from the leading point on the contact patch to the point of maximum deflection. In 1966, Pacejka[4] followed this by considering the contact line to have a number of different shapes. He implemented this tyre model in various ground vehicles, making use of experimental data and mathematical modelling. Instead of using a set curve for the contact line, Segel[5] allowed it to vary dynamically, thus modelling the actual shape of the contact patch. He called this the exact stretched-string model. In the 1990s, Somieski[6] developed a nose landing gear (NLG) model that consisted of the torsional dynamics of the landing gear, the forces and moments of the gear and the elastic characteristics of the tyre described by the stretched string. He found that, with lower damping and increased velocity and vertical load, the system was more likely to experience shimmy oscillations. This was extended by Thota *et al*,[7] who introduced a non-zero rake angle to the landing gear model and then included a lateral bending degree of freedom (DOF), which coupled to the torsional DOF via the tyre.[8] Thota *et al* used bifurcation analysis to investigate the interaction of the DOFs and found that, in addition to the well known torsional oscillations, the system may experience stable lateral and quasiperiodic shimmy oscillations.

The model presented in the work by Thota *et al* was used as a basis for the coupled NLG-fuselage model developed by Terkovics *et al*,[9] who added a lateral rigid body fuselage mode representing the displacement of the aircraft at the NLG-fuselage attachment point. They found that the presence of the fuselage affects the NLG shimmy dynamics significantly and, thus, the onset of shimmy is altered with the inclusion of their simple fuselage representation. As well as the rigid body modes, the flexible modes of the fuselage are also

important. Luber *et al*[10] investigated the effects of a fighter aircraft during its development phase. They found that the elastic fuselage modes are important when the natural frequencies of the fuselage are similar to that of the NLG modes. Wright and Cooper[11] also looked at the effect of a flexible fuselage coupled to single DOF landing gear models. They measured the heave response of the system when the gears passed over a dip in the runway. They then repeated the analysis when including a flexible mode in the fuselage model. The results show a significant response at the natural frequency of the flexible modes, indicating that the dynamic response of the fuselage increases with the inclusion of flexible modes.

In this paper a coupled NLG-fuselage model is derived and analysed in order to further investigate the interaction between the NLG and the fuselage. The model derivation considers the NLG and the fuselage as two separate systems that are coupled via constraint forces.

The fuselage model is a two DOF mass spring damper system in the lateral and vertical directions at the NLG-fuselage attachment point. The lateral displacement represents any modal characteristics of an elastic fuselage, and any yawing of a rigid fuselage whilst on the runway. The vertical fuselage displacement also represents the modal dynamics of an elastic fuselage, and any pitching of a rigid fuselage during ground manoeuvres. These generalisations are made because the amplitudes of the oscillations of the fuselage are assumed to be small and, therefore, can be modelled as linear translations. The NLG model is highly nonlinear; it models the torsional and lateral bending modes of the gear, which are coupled due to the geometry of the structure and via the tyre model, for the lateral deflection of the tyre.

This coupled model is studied by means of bifurcation analysis; results are presented as time histories and one- and two-parameter bifurcation diagrams. The bifurcation diagrams are created with the software package AUTO,[12] which has been integrated into Matlab via the Dynamical Systems Toolbox.[13] One-parameter bifurcation diagrams show that, when the forward velocity of the aircraft is increased, the straight-rolling solution becomes unstable via a Hopf bifurcation. The system then experiences stable periodic oscillations dominated by either the torsional or lateral modes of the NLG. Two-parameter bifurcation diagrams show the effect of fuselage motion on the dynamics of the NLG. Analysis shows that the two fuselage DOFs do affect the onset of shimmy oscillations and, in the shimmy region, their frequency and amplitude. Moreover, the onset of shimmy is influenced most by the fuselage when the lateral fuselage mode has a low effective mass. The vertical fuselage mode is found to have no effect on the onset of shimmy, but it influences the

severity of the oscillations once in the shimmy region.

The model is presented in section II, and the results in section III. In particular, bifurcation analysis in two parameters is carried out in subsection IIIC. Finally, conclusions are drawn in section IV.

II. Derivation of NLG-fuselage model

Since many of the landing gear models that are presented in the literature assume that the fuselage motion is negligible, we first concentrate on the landing gear model, including motion and forces at the interface with the fuselage. This model has four degrees of freedom, the torsional and lateral bending rotations of the landing gear and the lateral and vertical motions at the interface with the fuselage, ψ, δ, y_A and z_A respectively (see figure 1). The fuselage model is then discussed, introducing two additional degrees of freedom: a lateral and a vertical deflection, y and z respectively. The two subsystems are then combined to give the overall dynamics of the coupled fuselage and nose landing gear. At this stage the constraint that the tyre remains in contact with the ground is introduced, eliminating the z_A degree of freedom, resulting in a five degree of freedom model which is expressed in state-space form. Finally the tyre is considered, which introduced an additional state, λ.

The NLG is shown schematically in figure 1(a) and consists of a strut, caster and wheel, which have a

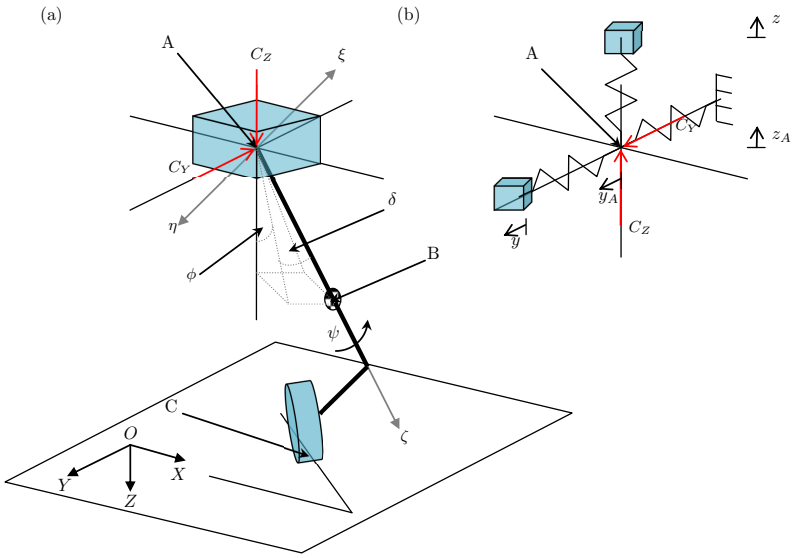

Figure 1. Schematic of coupled nose landing gear and fuselage model.

combined centre of gravity located at point B on the strut. The NLG is attached to the fuselage at point A and is in contact with the ground at point C. Two different coordinate frames are considered: a global frame with origin O is fixed to the ground and has orthogonal axes X, Y and Z, with the Z axis orientated vertically downwards and X axis pointing in the forward direction of the aircraft; and a moving (or body) frame, with its origin at point A and axes ξ, η and ζ. The ζ-axis is rotated from the vertical by the constant rake angle ϕ and is in-line with the strut in the downwards direction, while the ξ-axis is in-line with the caster. The NLG model has three DOFs. It is allowed to rotate torsionally about the ζ-axis by the angle ψ and to rotate through the lateral bending angle δ, about a rotated X-axis through A. Finally, the NLG is allowed to move laterally and vertically at point A by displacements y_A and z_A, respectively. The vertical displacement z_A, however, does not manifest itself as a degree of freedom due to ground constraints. The lateral displacement y_A is under no constraint but is grounded via a small compliance to remove rigid body drift. **Here, a single wheel gear is considered, with the gyroscopic effects neglected as the focus of the work is the effect of fuselage motion on the onset of shimmy. The effect of multiple wheels and their gyroscopic effects on the landing gear dynamics are reported by Thota *et al.*[14]**

A. The NLG model

Lagrangian mechanics were used to derive the equations of motion (EOMs) for this NLG system. **Along with the three DOFs (δ, ψ and y_A), the vertical displacment z_A is temporarily treated as a DOF.** For each DOF the Lagrangian equation

$$\frac{\partial}{\partial t}\left(\frac{\partial \mathcal{L}}{\partial \dot{q}_i}\right) - \frac{\partial \mathcal{L}}{\partial q_i} + \frac{\partial \mathcal{R}}{\partial \dot{q}_i} = Q_i \tag{1}$$

holds where $\mathcal{L} = T - U$, and T and U are the kinetic and potential energies of the system, respectively. Moreover, $\mathcal{R}$ is Rayleigh's dissipation function, Q_i is the expression for the generalised forces **and** $q_i = \delta, \psi, y_A$ **and** z_A **are the generalised coordinates.** The kinetic energy is given by

$$T = \frac{1}{2}\left(m \mid \mathbf{v}_B \mid^2 + \boldsymbol{\omega}^T J_B \boldsymbol{\omega}\right), \tag{2}$$

where the vector $\mathbf{v}_B$ is the velocity vector of point B, $\boldsymbol{\omega}$ is the angular velocity of the NLG about point A, m is the mass of the NLG and J_B is the inertia matrix tensor at point B in the global frame. The potential

energy and Rayleigh's dissipation function are defined by

$$U = \frac{1}{2}\left(k_\delta \delta^2 + k_\psi \psi^2 + k_{y_A} y_A^2\right) \tag{3}$$

and

$$\mathcal{R} = \frac{1}{2}\left(c_\delta \dot{\delta}^2 + c_\psi \dot{\psi}^2\right), \tag{4}$$

respectively, where k_ν and c_ν are the stiffness and damping coefficients of DOF ν. We can now show how the terms in equation (2) are derived.

Firstly, due to the coupling with the fuselage, it is convenient to write the EOMs in the global frame. As the transformation from the global frame to the body frame is via three successive rotations (ϕ, δ, ψ), a transformation matrix can be written, which transforms vectors expressed in the body frame to the global frame; it is given by

$$H = \begin{bmatrix} \cos\phi\cos\psi + \sin\phi\sin\delta\sin\psi & -\cos\phi\sin\psi + \sin\phi\sin\delta\sin\psi & \cos\delta\sin\phi \\ \cos\delta\sin\phi & \cos\delta\cos\psi & -\sin\delta \\ -\sin\phi\cos\psi + \cos\phi\sin\delta\sin\psi & \sin\phi\sin\psi + \cos\phi\sin\delta\cos\psi & \cos\delta\cos\phi \end{bmatrix}. \tag{5}$$

The position and velocity of point A in the global frame is given by

$$\mathbf{r}_A = \begin{bmatrix} Vt \\ y_A \\ -L - z_A \end{bmatrix} \tag{6}$$

and $\mathbf{v}_A = \dot{\mathbf{r}}_A$, respectively, where V is the constant forward velocity of the aircraft, t is time, and $L = l_g + R\cos\phi$ is the height of the NLG at equilibrium; l_g is the distance from point A to the end of the strut and R is the radius of the wheel. The position vector of point B in the body frame is given by

$$\mathbf{r}^b_{AB} = \begin{bmatrix} 0 \\ 0 \\ l_\zeta \end{bmatrix}, \tag{7}$$

where l_ζ is the distance of point B from point A at equilibrium. This can be transformed to the global frame by using the Euler transformation matrix in equation (5), giving the relative position of point B with respect to point A in the global frame as

$$\mathbf{r}_{AB} = H\mathbf{r}^b_{AB}. \tag{8}$$

Therefore, the absolute position of point B in the global frame is

$$\mathbf{r}_B = \mathbf{r}_A + \mathbf{r}_{AB} \tag{9}$$

and the absolute velocity is given by

$$\begin{aligned} \mathbf{v}_B &= \mathbf{v}_A + \mathbf{v}_{AB} \\ &= \begin{bmatrix} V - \sin\phi \sin\delta l_\zeta \dot{\delta} \\ \dot{y}_A - \cos\delta l_\zeta \dot{\delta} \\ -\dot{z}_A - \cos\phi \sin\delta l_\zeta \dot{\delta} \end{bmatrix}, \end{aligned} \tag{10}$$

where $\mathbf{v}_{AB} = \dot{\mathbf{r}}_{AB}$. Due to the successive rotations between the global frame and the body frame, the angular velocity vectors do not create an orthogonal set. Therefore, to transform the vectors into the global frame the rotation matrices must be applied individually, giving the angular velocity

$$\boldsymbol{\omega} = \begin{bmatrix} \cos\phi\dot{\delta} + \sin\phi\cos\delta\dot{\psi} \\ -\sin\delta\dot{\psi} \\ -\sin\phi\dot{\delta} + \cos\phi\cos\delta\dot{\psi} \end{bmatrix} \tag{11}$$

of the NLG with respect to point A.

As previously mentioned, the constraint at the ground leads to the variable z_A being constrained. An expression for z_A is found by calculating the velocity at the ground contact point; point C in figure 1(a). First, the position vector of point C in the body frame is given by

$$\mathbf{r}^b_{AC} = \begin{bmatrix} -e - R\sin\phi \\ 0 \\ l_g + R\cos\phi \end{bmatrix}, \tag{12}$$

where e is the caster length. Therefore, the absolute position of point C in the global frame is

$$\mathbf{r}_C = \mathbf{r}_A + \mathbf{r}_{AC}, \tag{13}$$

where $\mathbf{r}_{AC} = H\mathbf{r}^b_{AC}$. The absolute velocity of point C is

$$\mathbf{v}_C = \dot{\mathbf{r}}_C. \tag{14}$$

The ground constraint states that the gear must not lift off the ground. Therefore, the velocity at the ground in the Z direction equals 0, which yields the equation,

$$-\dot{z}_A + \dot{r}_{AC.Z} = 0. \tag{15}$$

Equation (15) gives an expression for the constrained variable $\dot{z}_A$. Finally, in order to calculate generalised forces Q_i, the forces acting on the landing gear must be defined. There are two forces acting in the Y and Z direction at point A, which couple the landing gear to the fuselage; they are given by

$$\mathbf{C}_{Y.NLG} = \begin{bmatrix} 0 \\ C_Y \\ 0 \end{bmatrix} \text{ and } \mathbf{C}_{Z.NLG} = \begin{bmatrix} 0 \\ 0 \\ C_Z \end{bmatrix} \tag{16}$$

and are indicated in figure 1(a). There are also gravitational forces at points A and B, given by

$$\mathbf{G}_A = \begin{bmatrix} 0 \\ 0 \\ Mg \end{bmatrix} \text{ and } \mathbf{G}_B = \begin{bmatrix} 0 \\ 0 \\ mg \end{bmatrix}, \tag{17}$$

respectively, where M is the static mass of the fuselage acting on the nose gear and g is the gravitational acceleration. At point C, there is a lateral tyre force and a vertical force given by the vectors

$$\mathbf{F}_Y = \begin{bmatrix} -F_z \Lambda \sin\theta \\ F_z \Lambda \cos\theta \\ 0 \end{bmatrix} \text{ and } \mathbf{F}_Z = \begin{bmatrix} 0 \\ 0 \\ -F_z \end{bmatrix}, \tag{18}$$

where θ is the ground projection of the angle ψ and is defined $\theta = \psi \cos\phi \cos\delta$. **The lateral tyre force is a function of Λ which is defined by**

$$\Lambda = k_\lambda \tan^{-1}(7\tan(\alpha)) \cos(0.95 \tan^{-1}(7\tan(\alpha))). \tag{19}$$

where k_λ is the restoring coefficient of the tyre, $\alpha = \tan^{-1}\left(\frac{\lambda}{L}\right)$ is the slip angle, L is the relaxation length and λ is the lateral displacement of the tyre. The definition of Λ is taken from Thota *et al*[8] which is based on work by Pacejka[15]. In addition, the landing gear experiences a self-aligning

moment due to the tyre, given by

$$\mathbf{M}_{k_\alpha} = \begin{bmatrix} 0 \\ 0 \\ -F_z C_{k_\alpha} \end{bmatrix}, \tag{20}$$

where

$$C_{k_\alpha} = \begin{cases} k_\alpha \frac{\alpha_m}{\pi} \sin\left(\alpha \frac{\pi}{\alpha_m}\right), & \text{if } |\alpha| \leq \alpha_m, \\ 0, & \text{if } |\alpha| > \alpha_m. \end{cases} \tag{21}$$

Here α_m is the maximum slip angle and k_α is the self-aligning coefficient of the tyre. This piecewise function is based on that in Somieski.[6]

The power P of the system is calculated by using the general expression

$$P = \sum_{j=1}^{N} \mathbf{F}_j \cdot \mathbf{v}_j + \sum_{k=1}^{M} \mathbf{M}_k \cdot \boldsymbol{\omega}_k = \sum_{i=1}^{n} Q_i \dot{q}_i \tag{22}$$

and the generalised forces for each coordinate are

$$Q_i = \sum_{j=1}^{N} \mathbf{F}_j \cdot \frac{\partial \mathbf{v}_j}{\partial \dot{q}_i} + \sum_{k=1}^{M} \mathbf{M}_k \cdot \frac{\partial \boldsymbol{\omega}_k}{\partial \dot{q}_i} \tag{23}$$

where $\mathbf{F}_j$ are the forces and $\mathbf{M}_k$ the moments acting on the system and $\mathbf{v}_j$ and $\boldsymbol{\omega}_k$ are the corresponding velocities respectively. Noting that the forces do not depend on velocity this can be rewritten as

$$Q_i = \frac{\partial P}{\partial \dot{q}_i} \tag{24}$$

to find the generalised forces of the system.

Equation (1), with DOFs $i = \delta, \psi, y_A, z_A$, in turn, can now be used to calculate the four equations of motion

for the landing gear

$$G_1\left(\ddot{\delta},\ddot{\psi},\ddot{y}_A,\ddot{z}_A\right)+G_2\left(\dot{\psi}^2,\dot{\delta}\dot{\psi}\right)+c_\delta\dot{\delta}+G_3F_z+k_\delta\delta+G_4 = 0, \tag{25}$$

$$H_1\left(\ddot{\delta},\ddot{\psi}\right)+H_2\dot{\delta}^2+c_\psi\dot{\psi}+H_3F_z+k_\psi\psi = 0, \tag{26}$$

$$J_1\left(\ddot{\delta},\ddot{y}_A\right)+J_2\dot{\delta}^2+J_3F_z+k_{y_A}y_A+C_Y = 0, \tag{27}$$

$$K_1\left(\ddot{\delta},\ddot{z}_A\right)+K_2\dot{\delta}^2-F_z+C_Z+mg = 0. \tag{28}$$

The coefficients $G_{1\ldots4}, H_{1\ldots3}, J_{1\ldots3}$ and $K_{1,2}$ are given in the Appendix.

B. The fuselage model

A schematic of the fuselage model is shown in figure 1(b). Once again, the attachment point between the fuselage and landing gear is labelled A. The fuselage is allowed to move laterally via the displacement y and vertically via the displacement z. These displacements have effective masses μ and ν, respectively. Equation (1) can be used again to calculate the equations of motion. The kinetic energy is given by

$$T=\frac{1}{2}\left(\mu\mid\mathbf{v}_\mu\mid^2+\nu\mid\mathbf{v}_\nu\mid^2\right), \tag{29}$$

where vectors $\mathbf{v}_\mu$ and $\mathbf{v}_\nu$ are the respective absolute velocity vectors in the global frame of effective masses μ and ν, given by

$$\mathbf{v}_\mu=\begin{bmatrix}0\\ \dot{y}_A+\dot{y}\\ 0\end{bmatrix} \text{ and } \mathbf{v}_\nu=\begin{bmatrix}0\\ 0\\ -\dot{z}_A-\dot{z}\end{bmatrix}. \tag{30}$$

The potential energy of the system and Rayleigh's dissipation function are given by

$$U=\frac{1}{2}\left(\mu {f_y^n}^2y^2+\nu {f_z^n}^2z^2\right) \text{ and } \mathcal{R}=\frac{1}{2}\left(2q\mu f_y^n\dot{y}^2+2s\nu f_z^n\dot{z}^2\right), \tag{31}$$

respectively, where f_y^n and f_z^n are the natural frequencies, and q and s are the relative dampings of the lateral and vertical fuselage modes. The fuselage has forces equal and opposite to those in equation (16),

given by

$$\mathbf{C}_{Y.F} = \begin{bmatrix} 0 \\ -C_Y \\ 0 \end{bmatrix} \text{ and } \mathbf{C}_{Z.F} = \begin{bmatrix} 0 \\ 0 \\ -C_Z \end{bmatrix}. \tag{32}$$

The generalised forces arise solely from the constraint forces and are calculated using equation (24). Implementing equation (1) for $i = y_A, z_A, y, z$ gives the equations of motion for the fuselage

$$\mu(\ddot{y}_A + \ddot{y}) + C_Y = 0, \tag{33}$$

$$\nu(\ddot{z}_A + \ddot{z}) - C_Z = 0, \tag{34}$$

$$\mu(\ddot{y}_A + \ddot{y}) + c_y\dot{y} + k_y y = 0, \tag{35}$$

$$\nu(\ddot{z}_A + \ddot{z}) + c_z\dot{z} + k_z z = 0. \tag{36}$$

C. Coupled NLG-fuselage model

Now that the NLG and the fuselage systems have been derived, they can be combined by eliminating the coupling force terms C_Y and C_Z. By using equations (27) and (33), C_Y is eliminated to give

$$M_1\left(\ddot{\delta}, \ddot{y}_A, \ddot{z}_A, \ddot{y}\right) + J_2\dot{\delta}^2 + J_3F_z + k_{y_A}y_A = 0. \tag{37}$$

Similarly, C_Z is eliminated by using equations (28) and (34) to give

$$R_1\left(\ddot{\delta}, \ddot{z}_A, \ddot{z}\right) + K_2\dot{\delta}^2 - F_z + Mg + mg = 0, \tag{38}$$

where M_1 and R_1 are given in the Appendix. Equation (38) can be rearranged to get an expression for F_z. The relationship $-\dot{z}_A + \dot{r}_{AC.Z} = 0$ is due to the ground constraint and is given in equation (15). These expressions for F_z and $\ddot{z}_A$ can be substituted into equations (25), (26), (35), (36) and (37) to give the five equations of motion for the overall NLG-2DOF fuselage model.

D. Tyre Model

The tyre model is based on the stretched-string model described by Dietrich and Von Schlippe.[3] The following derivation results in a kinematic expression for the lateral deformation of the tyre's leading contact point. Here, we assume that the tyre fully adheres to the ground at all times. Segel[5] defines the exact stretched-string model, where the actual shape of the

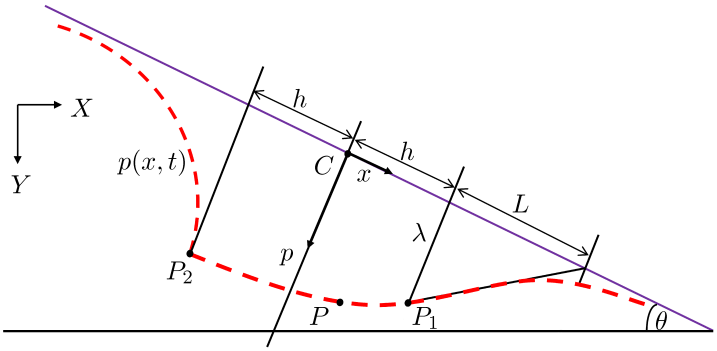

Figure 2. Deformation of the tyre described by the stretched-string model.

tyre contact line is considered. This contact line is defined by the function $p(x,t)$, $x \in [-h,h]$ and is shown in figure 2 where h is half the tyre contact patch length and L is the relaxation length. Therefore, the lateral tyre deflection $p(t)$ is described for any point P between the tyre's leading point P_1, and its trailing point P_2. If we consider point P on the curve $p(x,t)$, its absolute position vector is given in the global frame as a superposition of the absolute position of point C, the ground contact point (indicated in figures 1a and 2) and is defined as

$$\mathbf{r}_P = \mathbf{r}_C + \mathbf{r}_{CP} = \begin{bmatrix} r_{C.X} + x\cos\theta - p(x,t)\sin\theta \\ r_{C.Y} + x\sin\theta + p(x,t)\cos\theta \\ r_{C.Z} \end{bmatrix}, \tag{39}$$

where $r_{C.X}$, $r_{C.Y}$ and $r_{C.Z}$ are the X, Y, and Z components of the position vector $\mathbf{r}_C$ given in equation (13). Its velocity vector is thus

$$\mathbf{v}_P = \dot{\mathbf{r}_P} = \begin{bmatrix} \dot{r}_{C.X} + \dot{x}\cos\theta - x\dot{\theta}\sin\theta - (p'(x,t)\dot{x} + \dot{p}(x,t)) - p(x,t)\dot{\theta}\cos\theta \\ \dot{r}_{C.Y} + \dot{x}\sin\theta + x\dot{\theta}\cos\theta + (p'(x,t)\dot{x} + \dot{p}(x,t)) - p(x,t)\dot{\theta}\sin\theta \\ \dot{r}_{C.Z} \end{bmatrix}. \tag{40}$$

The condition that the tyre fully adheres to the ground implies that the velocity of point P is 0. Therefore, enforcing the condition $\mathbf{v}_P = \mathbf{0}$ gives the following constraint equations

$$\dot{r}_{C.X} + \dot{x}\cos\theta - x\dot{\theta}\sin\theta - (p'(x,t)\dot{x} + \dot{p}(x,t)) - p(x,t)\dot{\theta}\cos\theta = 0, \tag{41}$$

$$\dot{r}_{C.Y} + \dot{x}\sin\theta + x\dot{\theta}\cos\theta + (p'(x,t)\dot{x} + \dot{p}(x,t)) - p(x,t)\dot{\theta}\sin\theta = 0, \tag{42}$$

$$\dot{r}_{C.Z} = 0. \tag{43}$$

Equation (43) gives us the expression for our constrained variable $\dot{z}_A$ already given in equation (15). Equations (41) and (42) can be solved for $\dot{p}(x,t)$;

$$\dot{p}(x,t) = \dot{r}_{C.X}\sin\theta - \dot{r}_{C.Y}\cos\theta - x\dot{\theta} - p'(x,t)\left(p\dot{\theta} - \dot{r}_{C.X}\cos\theta - \dot{r}_{C.Y}\sin\theta\right) \tag{44}$$

to give a constraint of the lateral displacement of point P along the contact line. This PDE can be coupled to the equations of motion; the reader is directed to work by Takacs *et al.*[16] However, here we choose to approximate the constraint equation to consider the lateral displacement at the leading contact point P_1 only; namely where $x = h$, and assume that no sliding occurs in the contact area. This could lead to a 'kink' in the contact line at points P_1 and P_2. We can assume that when rolling the string forms a continuous varying slope at point P_1 whilst at point P_2 there may be discontinuities due to the absence of bending stiffness. For further explanation and proof of this, see Pacejka.[15] As the slope is continuous at the leading point, it can be written as

$$p'(x,t)\mid_{x=h} = -\frac{\lambda(t)}{L}. \tag{45}$$

Using this, equation (44) becomes an ODE that describes the kinematics of the tyre at the contact leading point via

$$\dot{\lambda}(t) = \dot{r}_{C.X}\left(\sin\theta - \frac{\lambda(t)}{L}\cos\theta\right) - \dot{r}_{C.Y}\left(\cos\theta + \frac{\lambda(t)}{L}\sin\theta\right) - \left(h - \frac{\lambda(t)^2}{L}\right)\dot{\theta}. \tag{46}$$

This first-order differential equation, along with the five second-order differential equations (equations (25), (26), (35), (36) and (37), once equation (38) and (15) are used to eliminate F_z and $\ddot{z}_A$) represent the coupled NLG-2DOF fuselage model.

III. Bifurcation analysis of NLG-fuselage model

The parameter values used for the nose landing gear model presented in section II are shown in table 1; they are mostly taken from Thota *et al.*[8] The parameter values for the fuselage model are shown in table 2 and are chosen in a realistic range to ensure that the system exhibits shimmy; i.e. the vertical load is reasonably large.

A. Examples of shimmy oscillation

The existence of shimmy in the NLG-fuselage system can be shown by numerically integrating the equations of motion with respect to time given in section II. Figures 3 and 4 show example time responses for the DOFs ψ, δ, y and z and their corresponding frequency spectra; parameter values remain constant during each time history. Figure 3 shows the system experiencing shimmy at a velocity of $V = 50$m/s. It can be seen that all DOFs display oscillatory motion; however, some are more responsive than others. The maximum amplitude of the torsional angle, ψ, is very large compared to that of the lateral bending angle, δ; hence, we refer to this as *torsionally dominated shimmy*. It can also be seen that the maximum amplitudes of the lateral fuselage and vertical fuselage DOFs (y and z, respectively) are small and not overly responsive in this type of shimmy. A further point to note is that the DOFs ψ, δ, λ and y are locked into a frequency of 11Hz, while the vertical fuselage DOF oscillates at a frequency of 22Hz, double that of the other DOFs.

Figure 4 shows the system experiencing a second type of shimmy at velocity $V = 50$m/s. The maximum torsional angle, ψ, is now much smaller and the maximum lateral bending angle, δ, is much larger; this indicates that the shimmy experienced at this velocity is dominated by lateral bending, and it is referred to as *laterally dominated shimmy*. It can be seen that the lateral fuselage DOF is much more responsive to this type of shimmy compared to that in figure 3. The maximum amplitude of the vertical fuselage DOF is slightly larger in figure 4, but still small. The DOFs δ, ψ, λ and y oscillate at a frequency of 15Hz and once again the vertical fuselage DOF, z, oscillates at 30Hz, double that of the other DOFs.

We observe that both time series were taken at $V = 50$m/s, indicating that the system has two stable periodic solutions at this velocity and can, therefore, experience either torsionally dominated shimmy or laterally dominated shimmy depending on the initial conditions.

Table 1. NLG and tyre parameters

Parameter	Name	Value	Units
NLG data			
l_ζ	distance from A to B	1.25	m
m	mass of the landing gear	320	kg
$J_{\zeta\zeta}$	m.m. of inertia at B with respect to ζ-axis	100	kg m^2
$J_{\xi\xi}$	m.m. of inertia at B with respect to ξ-axis	100	kg m^2
$J_{\eta\eta}$	m.m. of inertia at B with respect to η-axis	100	kg m^2
$J_{\xi\eta}$	p. of inertia at B with respect to (ξ,η)-axes	0	kg m^2
$J_{\xi\zeta}$	p. of inertia at B with respect to (ξ,ζ)-axes	0	kg m^2
$J_{\eta\zeta}$	p. of inertia at B with respect to (η,ζ)-axes	0	kg m^2
k_δ	lateral stiffness of strut	6.1E6	Nm rad^{-1}
c_δ	lateral damping of strut	300	Nms rad^{-1}
k_ψ	torsional stiffness of strut	3.8E5	Nm rad^{-1}
c_ψ	torsional damping of strut	300	Nms rad^{-1}
l_g	distance from point A to the end of the strut	2.138	m
ϕ	rake angle	9	$^\circ$
Tyre and wheel data			
R	wheel radius	0.362	m
L	relaxation length	0.3	m
e	caster length	0.12	m
k_λ	restoring coefficient of the tyre	0.002	rad^{-1}
h	half contact patch length	0.1	m
k_α	self-aligning coefficient of the tyre	1.0	m rad^{-1}
α_m	self-aligning moment limit	10	$^\circ$
Other			
g	gravitational acceleration	9.81	m s^{-2}

B. One-parameter continuation

We now consider a one-parameter continuation with the forward velocity, V, as the continuation parameter. Figure 5 shows its projections onto the five variables ψ, δ, λ, y and z. The diagram shows the maximum

Table 2. Fuselage parameters

Parameter	Name	Value	Units
M	Fuselage mass at NLG	12	t
f_y^n	lateral natural frequency	15	Hz
f_z^n	vertical natural frequency	15	Hz
μ	lateral effective mass	2	t
ν	vertical effective mass	2	t
q	lateral relative damping	0.02	
s	vertical relative damping	0.02	

response amplitude of the system steady states for any value of V. The solution can either be stable or unstable. A stable solution can be either an equilibrium where the system is straight rolling (no shimmy), or a periodic orbit at constant amplitude (stable shimmy). Figure 5 shows that for low velocities the equilibrium (or straight-rolling) solution is stable. When the velocity is increased, the system experiences a supercritical Hopf bifurcation, H_t, at $V = 4.86$m/s. This causes the straight-rolling equilibrium to become unstable and gives rise to a stable periodic orbit whose maximum amplitude forms the black branch. From the projection of this branch in the maximum torsional angle (figure 5(a)), compared to that of the lateral bending angle (figure 5(b)), it is evident that this branch is torsionally dominated. Shimmy experienced along this branch will therefore be similar to that shown in the time series in figure 3. Following this branch as the forward velocity is increased further, the system experiences a torus bifurcation, T_t, at $V = 67.5$m/s. Here, the torsionally dominated branch loses stability, and the unstable branch then joins the unstable straight-rolling solution via a Hopf bifurcation, H_t', at $V = 69.9$m/s. After the straight-rolling solution initially loses stability via a Hopf bifurcation, H_t, it experiences a second Hopf bifurcation, H_l, at $V = 14.29$m/s. This Hopf bifurcation is subcritical, and the resulting branch is unstable. At $V = 41.3$m/s the branch gains stability via torus bifurcation, T_l. From observing its projection in the torsional and lateral bending angles, this branch can be identified as laterally dominated. Here, the shimmy is similar to that displayed in the time series in figure 4. This laterally dominated branch remains stable as the velocity is increased and joins the straight-rolling solution, which regains stability at a Hopf bifurcation, H_l', at $V = 77.17$m/s. As previously mentioned, the system has areas of bistability, where the shimmy experienced is dependent upon the choice

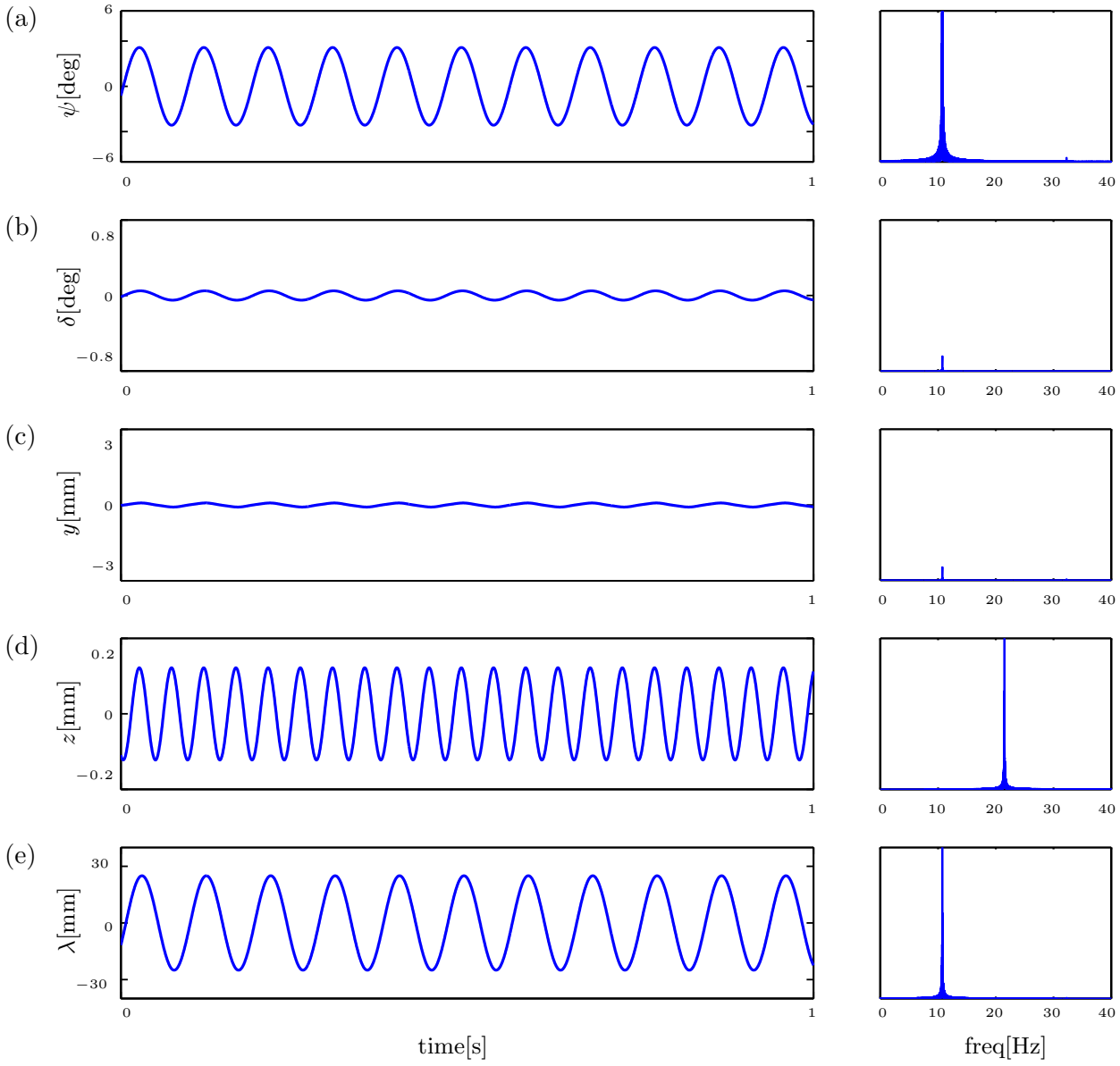

Figure 3. Time series of equations (25), (26), (35), (36) and (37) taken at forward velocity $V = 50$m/s showing the system exhibiting *torsionally dominated shimmy*; all other parameters are as in tables 1 and 2.

of initial conditions and it covers the interval $V \in [41.3, 76.5]$. This region of bistability is easily identified in the one-parameter continuation diagrams in figure 5.

C. Two-parameter continuations

The effect of the fuselage on the NLG can now be investigated by considering two-parameter continuations in which the bifurcation points from figure 5 are continued in a second parameter.

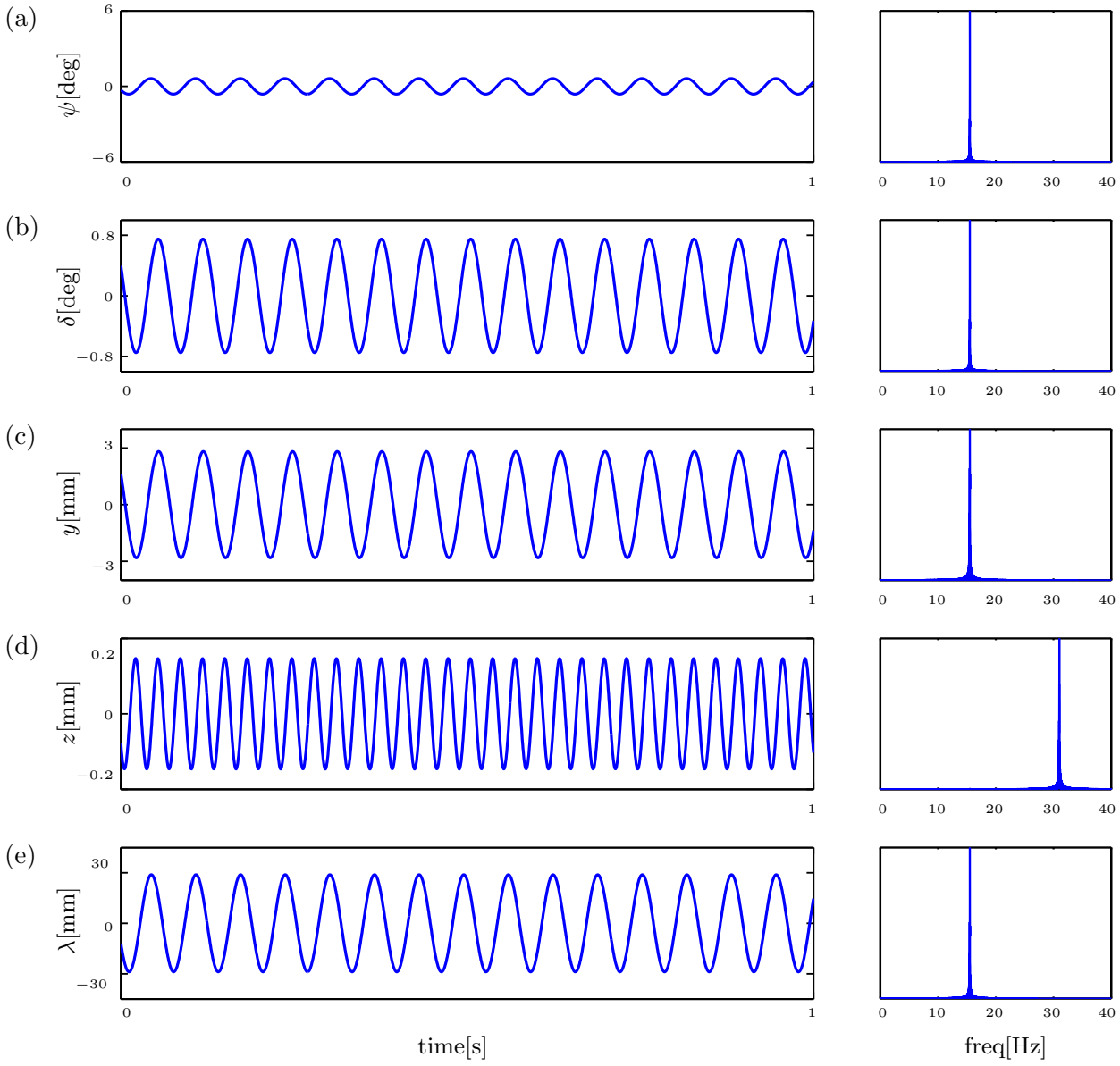

Figure 4. Time series of equations (25), (26), (35), (36) and (37) taken at forward velocity $V = 50$m/s showing the system experiencing *laterally dominated shimmy*; all other parameters are as in tables 1 and 2.

1. *Two-parameter bifurcation diagrams in the (V, M)-plane*

We first consider as the second continuation parameter the static mass, M of the fuselage acting on the NLG. Two resulting bifurcation diagrams in the (V, M)-plane with fuselage dynamics, and without, are shown in figure 6. Continuing the Hopf bifurcation points H_t and H_l in V and M results in the thick black curves H_t^c and H_l^c, respectively. Torus bifurcation points from figure 5, T_t and T_l, are also continued in these parameters and result in the grey curves T_t^c and T_l^c, respectively. We note here that the torus curves emerge

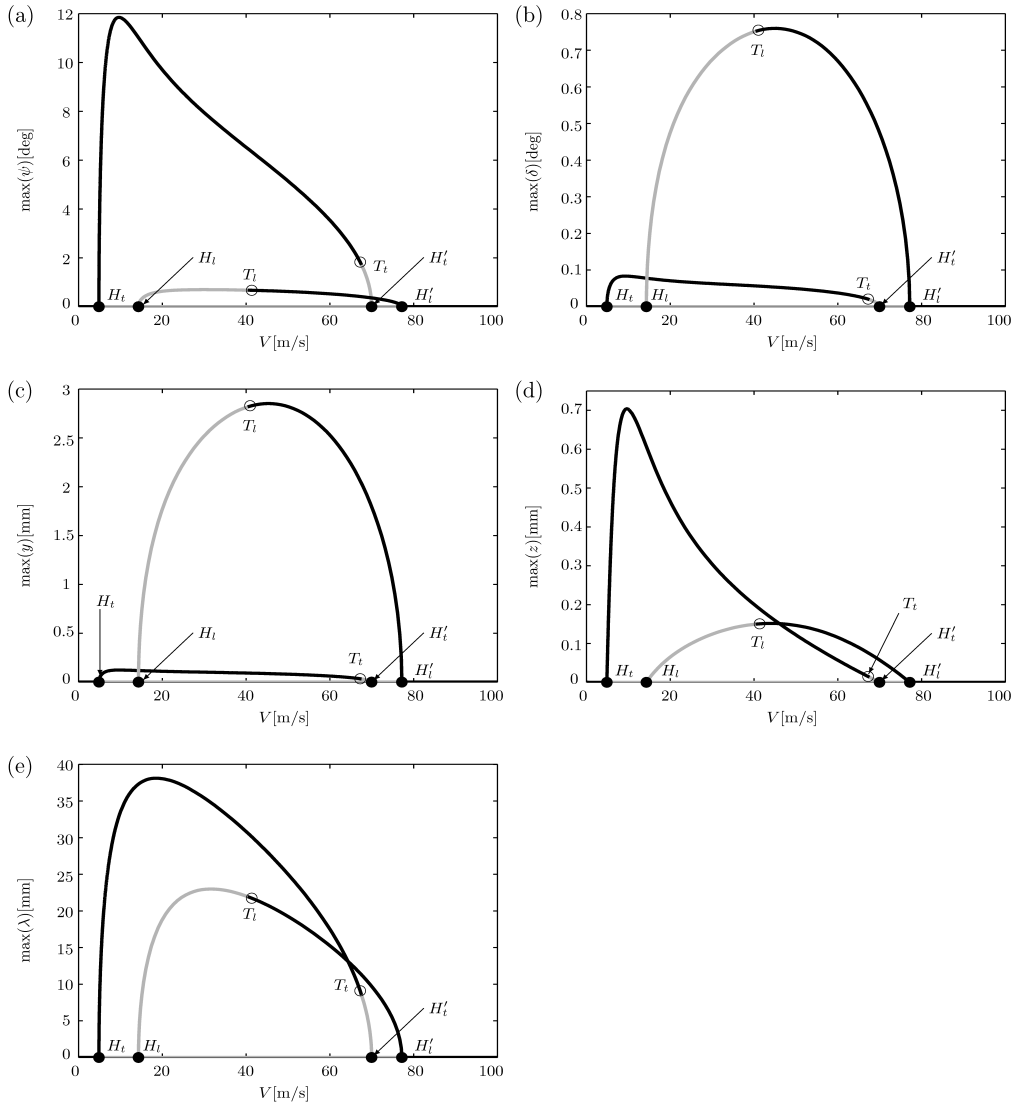

Figure 5. One-parameter bifurcation diagrams in V showing the maximum amplitudes of ψ, δ, λ, y and z for $M = 12$t; other parameters are as given in tables 1 and 2.

from intersection points of H_t and H_l known as double Hopf points, HH. The Hopf bifurcation curves are stability boundaries of the equilibrium solution and, therefore, indicate the onset of shimmy. The torus curves are stability boundaries of the periodic orbits; T_t^c for the torsional and T_l^c for the lateral shimmy oscillations. The bifurcation diagram shows that the straight-rolling solution is entirely stable in the unshaded area. Consistent with the one-parameter continuation in figure 5, over the given range of velocities, the system has regions of purely stable torsionally dominated shimmy, purely stable laterally dominated shimmy, as well as a region of bistability where the two stable periodic solutions co-exist and the type of shimmy experienced

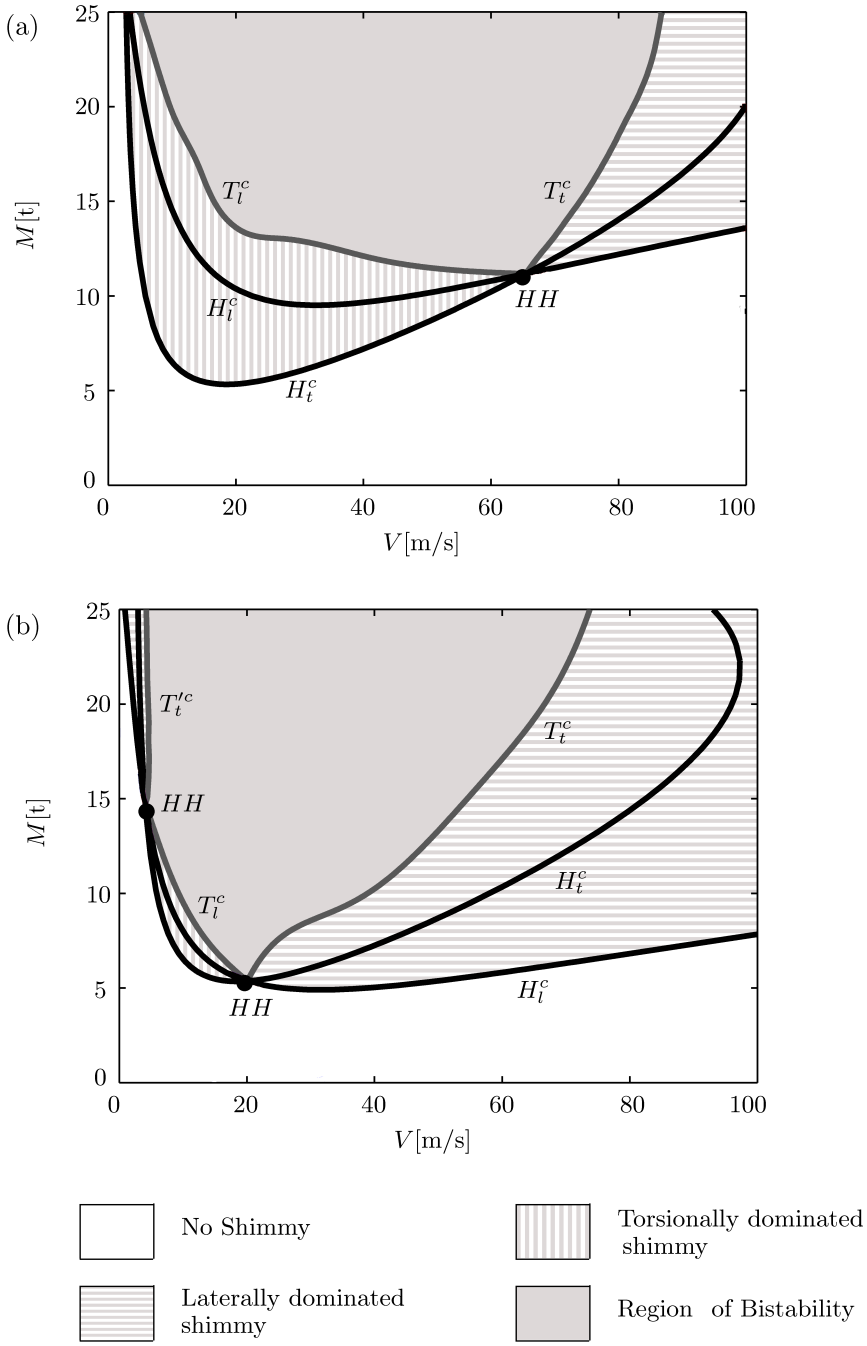

Figure 6. Two-parameter bifurcation diagrams in the (V, M)-plane for (a) an oscillating fuselage where parameters are as given in table 2, and (b) for a non-oscillating fuselage where $\mu = \nu = 10000$t.

depends upon the initial conditions. These regions are bounded by the shown bifurcation curves.

In figure 6(a) the system experiences torsionally dominated shimmy in the region bounded by the curves H_t^c and T_t^c. However, this region is split into two parts, in the part indicated by the vertically striped shading

and bounded by the curves H_l^c and T_l^c, there is only one periodic solution corresponding to the torsionally dominated shimmy. In the second part, indicated by the block grey shading and bounded by the curves T_l^c and T_t^c, there are two periodic solutions corresponding to torsionally and laterally dominated shimmy; this is the region of bistability. The region indicated by the horizontal shading and bounded by the curves H_l^c and T_l^c is the region of laterally dominated shimmy only. Note that the one-parameter continuation in figure 5 is a cross section of figure 6(a) at $M = 12$t.

In order to evaluate the effect of the fuselage modes on the landing gear stability, the fuselage masses are now set to very large values; this is the practical equivalent of setting them to infinity such that their dynamics is suppressed. Figure 6(b) shows the respective two-parameter bifurcation diagram in the (V, M)-plane with $\mu = \nu = 10000$t. It can be seen that the bifurcation curves have moved compared to those in figure 6(a), so there is a smaller region of the desirable straight-rolling solution. In particular, for intermediate to large values of V, the boundary of stability of the straight-rolling solution is lower in figure 6(b) and consists of a transition to laterally dominated shimmy. There is also a second double Hopf bifurcation point in figure 6(b) at $M \approx 15$t. It gives rise to a second torus bifurcation curve, $T_t'^c$, creating a second small region of purely laterally dominated shimmy. We remark figure 6(b) is in agreement with the findings in Thota *et al*[8] on a NLG without the consideration of the fuselage dynamics.

Overall figure 6(b) indicates that the oscillating fuselage stabilizes the gear, resulting in an increased region of stable straight-rolling, that is, no shimmy. This energy is transferred into the fuselage and dissipates, meaning that the fuselage acts as a passive damper in certain parameter regions. The differences between figure 6(a) and (b) clearly show that the fuselage influences the dynamics of the NLG. However, as the fuselage model is a two DOF system, it is unclear what effect each fuselage DOF has. We can investigate this by studying the effects of separately varying the different fuselage parameters, i.e. the respective effective mass and natural frequency.

2. Effect of the lateral fuselage DOF

By keeping the natural frequency and effective mass of the vertical DOF fixed at the values given in table 2, we can now investigate the effects of the lateral fuselage mode. To do this, we consider the two-parameter bifurcation diagrams in figure 7. In panel (a) the bifurcation diagram is shown in the (V, f_y^n)-plane, that

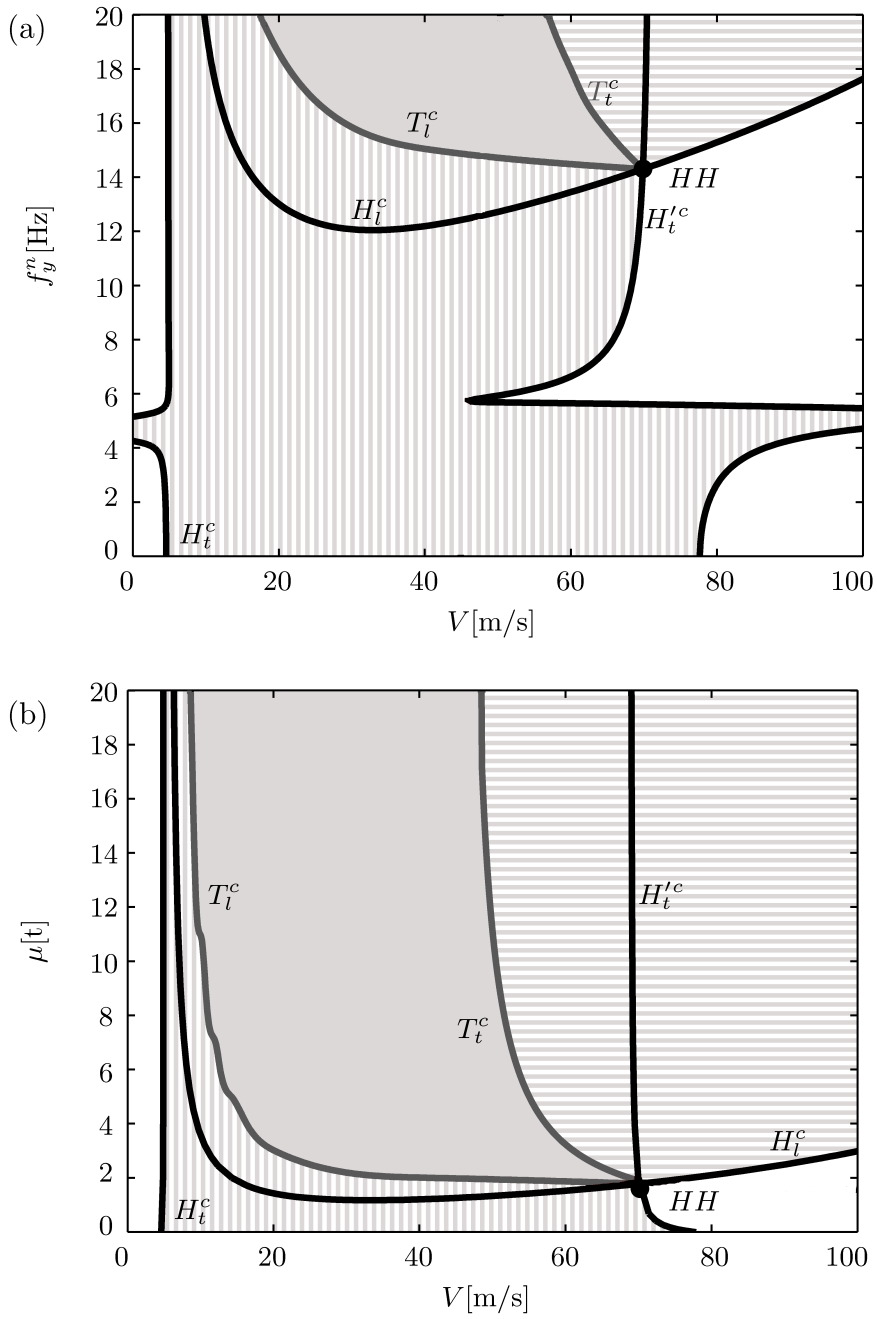

Figure 7. Two-parameter bifurcation diagrams, (a) in the (V, f_y^n)-plane and (b) in the (V, μ)-plane; shading reflects the type of shimmy, as defined in figure 6.

is, the two continuation parameters are the forward velocity V and the natural frequency f_y^n of the lateral fuselage DOF. Once again, the one-parameter continuation in figure 5 is a cross section of this bifurcation diagram; namely at $f_y^n = 15$Hz. The Hopf bifurcation curves that bound the stable and unstable areas of the equilibrium solution show that the boundaries of the shimmy region are influenced by the natural

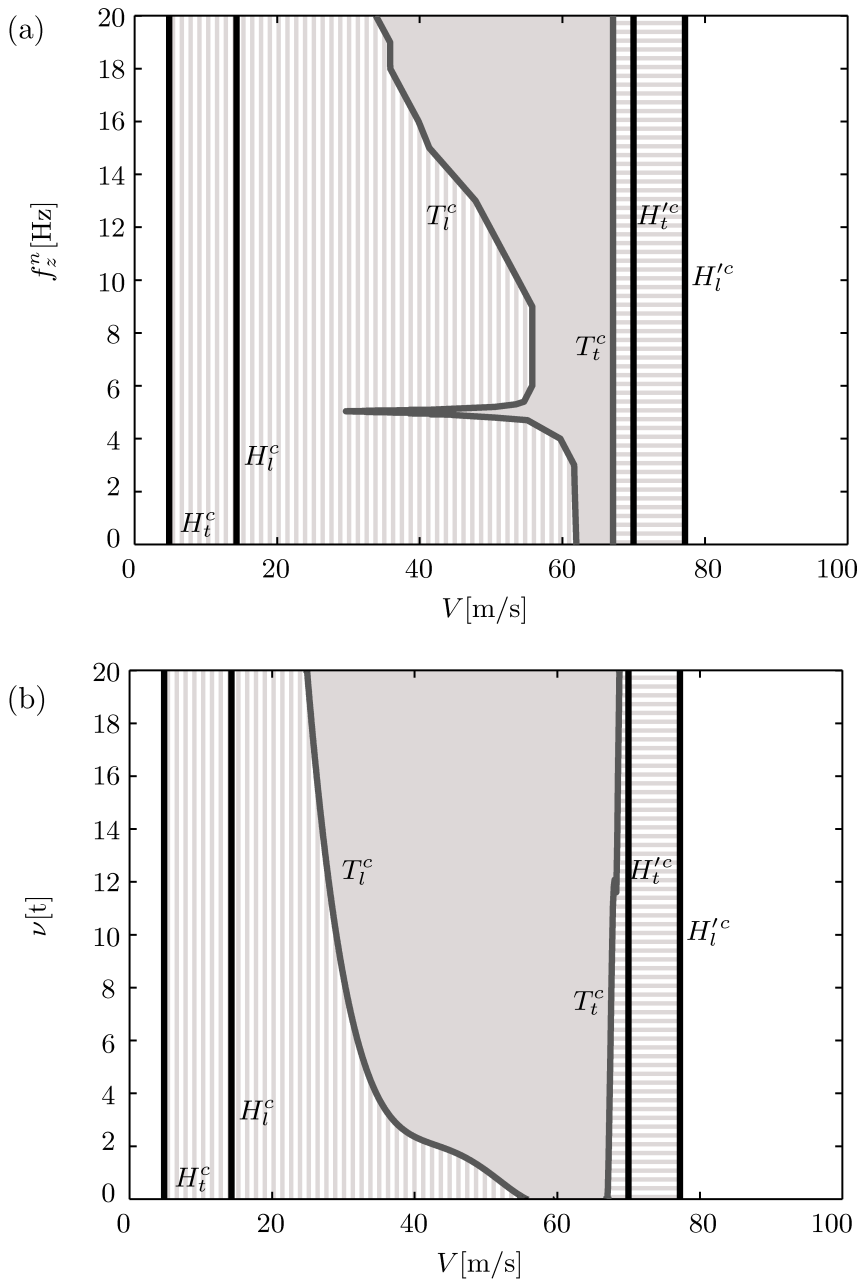

Figure 8. Two-parameter bifurcation diagrams, (a) in the (V, f_z^n)-plane and (b) in the (V, ν)-plane; shading reflects the type of shimmy, as defined in figure 6.

frequency. We observe that, for fuselage frequencies of $f_y^n < 15$Hz, the system experiences purely torsionally dominated shimmy. However, at $f_y^n = 14.3$Hz the Hopf bifurcation curves, H_l^c and $H_t'^c$, intersect at the double Hopf point HH, leading to emerging torus bifurcation curves, T_l^c and T_t^c, that give rise to stable laterally dominated shimmy. Therefore, for $f_y^n > 15$Hz, the system has regions of purely torsionally dom-

inated shimmy, regions of purely laterally dominated shimmy and regions of bistability. The introduction of laterally dominated shimmy at $f_y^n = 15$Hz shows that there is a resonance between the NLG and the fuselage, because the natural frequency of the gear's lateral bending mode is 15Hz. For $f_y^n = 5.2$Hz, the onset points of shimmy are highly affected by the presence of the fuselage dynamics. Since the natural frequency of the gear's torsional mode is 11Hz, the value of 5.2Hz is roughly half the natural frequency, indicating a 2:1 resonance between the fuselage lateral DOF and the nose gear.

Figure 7(b) shows the bifurcation diagram in the (V, μ)-plane, with the forward velocity V and the effective mass μ of the lateral DOF as the continuation parameters. The one-parameter continuation in figure 5 is a cross section at $\mu = 2$t. The Hopf bifurcation curves in panel (b) show that the effective mass has less of an impact on the onset of shimmy than the natural frequency; however lower effective mass values show a larger range of equilibrium stability for large velocity values. At these low values of μ, when the NLG does shimmy it does so purely torsionally. However, as the effective mass μ increases, other types of shimmy are introduced due to the intersection of the Hopf bifurcation curves H_t^c and H_l^c at the double Hopf point HH at $\mu \approx 2$t. The torus bifurcation curves, T_l^c and T_t^c, emerge from HH and the system has regions of both types of shimmy as well as bistability between them.

3. Effect of the vertical fuselage DOF

The same approach is now taken to investigate the effects of the vertical DOF. The natural frequency and effective mass of the lateral fuselage DOF are kept fixed at the values given in table 2. Figure 8 shows two-parameter bifurcation diagrams in the (V, f_z^n)-plane in panel (a) and in the (V, ν)-plane in panel (b). The one-parameter bifurcation diagrams in figure 5 are a cross section of the diagrams in figure 8(a) and 8(b) at $f_z^n = 15$Hz and $\nu = 2$t, respectively. The Hopf bifurcation curves, H_t^c and H_l^c, which bound the shimmy region in both panels (a) and (b), are invariant under the change in natural frequency and effective mass. This indicates that the onset of shimmy does not depend on the vertical DOF. However, the torus bifurcation curves, T_t^c and T_l^c, are sensitive to f_z^n and ν; this indicates that the vertical fuselage DOF affects the type of oscillatory behaviour in the shimmy region. We also note that in figure 8(a) the torus bifurcation curve T_l^c experiences a dip in velocity at $f_z^n = 5.1$Hz. This implies that there is a larger region of bistability

at this value of f_z^n than at other values. Similar to the lateral fuselage DOF, this could be due to 5Hz being roughly half the natural frequency of the torsional and lateral oscillations, suggesting a 2:1 resonance between the NLG and the vertical fuselage mode.

IV. Conclusions

A mathematical model has been developed to investigate the interaction between a NLG and the fuselage. This NLG model includes a torsional angle, ψ, and a lateral bending angle, δ. In addition, the gear is free to move laterally and vertically at the NLG-fuselage attachment point. Fuselage dynamics are included in the form of two translational DOFs. They represent the local displacement of the yaw and pitch dynamics of the fuselage about its centre of gravity and any movement from flexible modes of the fuselage. This coupled NLG 2DOF fuselage model is then completed by the exact stretched-string tyre model.

With this model the effects of the variation of fuselage parameters on stability and oscillatory characteristics of the NLG have been explored by means of a bifurcation analysis with respect to key parameters. The bifurcation diagrams presented were created with the bifurcation software package AUTO, as integrated into Matlab via the Dynamical Systems Toolbox. One-parameter bifurcation diagrams with the forward velocity of the aircraft as the continuation parameter identified stable branches of periodic orbits that correspond to stable, observable shimmy oscillations of the gear. We found that these branches can be dominated by either the torsional or lateral DOFs of the gear. They are bounded by bifurcation points which can be continued in two parameters to give a more global view of the dynamics of the system. Two-parameter bifurcation diagrams in the (V, M)-plane were considered, both with an oscillating fuselage and a fuselage of infinite mass. These showed that the presence of an oscillating fuselage increases the region where the straight-rolling solution is stable, suggesting that the presence of the fuselage stabilizes the gear. This indicates that energy is being transferred from the gear into the lateral fuselage mode, where it is dissipated.

We also investigated the effects of the two fuselage DOFs separately, which showed that the onset of shimmy is dependent upon the lateral but not the vertical fuselage DOF. This indicates that the increased area of the stable straight-rolling solution for the oscillating fuselage in the (V, M)-plane is due to the lateral fuselage DOF, and not the vertical one. The onset and decay of shimmy oscillations is affected most by the lateral fuselage DOF for natural frequency values of 5.2Hz and less than 14.3Hz and effective mass

values of approximately less than 4t. The system is therefore showing a resonance with the nose landing gear whose natural frequencies are 11Hz and 15Hz. While the vertical DOF does not appear to affect the onset of shimmy, it does however affect the system once it is oscillating. Overall the conclusion is that the interactions between the fuselage and the NLG exist; the fuselage can influence the dynamics of the gear during shimmy, and in the case of the lateral DOF, the onset of shimmy.

Future work on the landing gear model involves extending the model to include the axial compression of the strut and investigating gyroscopic effects of the wheel. Based on the demonstration here of the fuselage's influence on the NLG shimmy dynamics, the two DOF fuselage model can also be extended to further explore its effects on the NLG dynamics. The current fuselage model represents the motion of the fuselage as a local displacement at the NLG-fuselage attachment point. To further investigate the effects of fuselage dynamics on shimmy onset it would be of interest to extend the model to analyse the dynamics of the NLG when it is coupled to pitch, heave, yaw, roll, as well as flexible modes of the entire fuselage.

Acknowledgements

We thank Robert Jung, Tom Wilson and Etienne Coetzee from Airbus for helpful discussions and their support. Sarah Kewley is supported by an EPSRC and Airbus funded CASE studentship and Simon Neild by an EPSRC fellowship (EP/K005375/1).

References

[1]G. Broulhiet, The suspension of the automobile steering mechanism: shimmy and tramp (in French). *Bull Soc. Ing. civ. Fr.*, 78:540-554, 1925

[2]H. Fromm, Brief Report on the History of the Theory of Shimmy. *National Advisory Committee for Aeronautics*, *NACA TM 1365*, 1954

[3]B. von Schlippe and R. Dietrich, Shimmying of a pneumatic wheel. *National Advisory Committee for Aeronautics*, NACA TM 1365, 1947

[4]H.B. Pacejka, The wheel shimmy phenomenon: A theoretical and experimental investigation with particular reference to the nonlinear problem. *Dissertation, Delft University of Technology*, 1966

[5]L. Segel, Force and Moment Response of Pneumatic Tires to Lateral Motion Inputs. *Journal of Engineering for Industry*, Vol. 88, 1967. pp. 30-50. doi:10.1115/1.3670888

[6]G. Somieski, Shimmy analysis of a simple aircraft nose landing gear model using different mathematical methods.

Aerospace Science and Technology, (8):545-555, 1997 doi:10.1016/S1270-9638(97)90003-1

[7]P. Thota, B. Krauskopf and M. Lowenberg, Shimmy in a non-linear model of an aircraft nose landing gear with nonzero rake angle. *Proceedings of ENOC*, 2008

[8]P. Thota, B. Krauskopf and M. Lowenberg, Interaction of torsion and lateral bending in aircraft nose landing gear shimmy. *Nonlinear Dynamics*, 57(3), 2009. doi:10.1007/s11701-008-9455-y

[9]N. Terkovics, S. Neild, M. Lowenberg and B. Krauskopf, Bifurcation Analysis of a Coupled Nose-Landing-Gear-Fuselage-System. *Journal of Aircraft*, 2014. doi:10.2514/1.C032324

[10]W. Luber, G. Kempf and A. Krauss, Self Induced Oscillations of Landing Gear as an Integral Landing Gear Aircraft System Problem.*Advisory Group for Aerospace Research and Development*, AGARD-R-800, 1996

[11]J.R. Wright and J.E. Cooper. Introduction to Aircraft Aeroelasticity and Loads. *John Wiley & Sons*, 2007

[12]E.J. Doedel, with major contributions from A. Champneys, T. Fairgrieve, Yu. Kuznetsov, B. Oldeman, R. Paffenroth, B. Sandstede, X. Wang, and C. Zhang. Auto-07P: Continuation and bifurcation software for ordinary differential equations, 2008. available at http://indy.cs.concordia.ca/auto/

[13]E. Coetzee, B. Krauskopf and M. Lowenberg, The Dynamical Systems Toolbox: Integrating AUTO into Matlab, 16th US National Congress on Theoretical and Applied Mechanics. *State College, Pennsylvania*, 2010

[14]P. Thota, B. Krauskopf and M. Lowenberg, Multi-Parameter Bifurcation Study of Shimmy Oscillation in a Dual-Wheel Aircraft Nose Landing Gear. *Nonlinear Dynamics*, Vol.70, No2, 2012

[15]H. B. Pacejka, Tyre and Vehicle Dynamics. *Elsevier Butterworth-Heinemann*, 2nd edition, 2006

[16]D. Takacs, G. Stepan, Micro-shimmy of towed structures in experimentally uncharted unstable parameter domain. *Journal of Vehicle Mechanics and Mobility*, 50:11, 1612-1630, DOI:10.1080/00423114.2012.691522

A. Appendix

The functions and coefficients for the EOMs given in equations (25)-(28) are as follows, where we use the notation $C_x = \cos x$ and $S_x = \sin x$ for $x = \phi, \delta, \psi, \theta$:

For equation (25):

$$\begin{aligned} G_1 &= G_{11}\ddot{\delta} + G_{12}\ddot{\psi} + G_{13}\ddot{y}_A + G_{14}\ddot{z}_A, \\ G_2 &= G_{21}\dot{\psi}^2 + G_{22}\dot{\delta}\dot{\psi}, \\ G_3 &= S_\phi(r_{AC.X}\Lambda C_\theta + r_{AC.Y}\Lambda S_\theta - C_{k_\alpha}) + C_\phi(r_{AC.Z}\lambda C_\theta + r_{AC.Y}), \\ G_4 &= mgS_\delta C_\phi l_\zeta, \end{aligned}$$

where

$$
\begin{aligned}
G_{11} &= ml_\zeta^2 + J_{\xi\xi}C_\psi^2 + J_{\eta\eta}S_\psi^2 - 2J_{\xi\eta}S_\psi C_\psi, \\
G_{12} &= J_{\xi\zeta}C_\psi - J_{\eta\zeta}S_\psi, \\
G_{13} &= -mC_\delta l_\zeta, \\
G_{14} &= mS_\delta C_\phi l_\zeta, \\
G_{21} &= -\left(J_{\eta\zeta}C_\psi + J_{\xi\zeta}S_\psi\right), \\
G_{22} &= 2\left((J_{\eta\eta} - J_{\xi\xi})S_\psi C_\psi + J_{\xi\eta}S_\psi^2\right).
\end{aligned}
$$

For equation (26):

$$
\begin{aligned}
H_1 &= G_{12}\ddot{\delta} + H_{11}\ddot{\psi}, \\
H_2 &= (J_{\xi\xi} - J_{\eta\eta})S_\psi C_\psi + J_{\xi\eta}(C_\psi^2 - S_\psi^2), \\
H_3 &= S_\phi\left(r_{AC.Y}C_\delta + \Lambda r_{AC.Z}C_\delta C_\theta\right) + C_\phi\left(C_{k_\alpha}C_\delta - \Lambda S_\theta r_{AC.Y}C_\delta - \Lambda C_\theta r_{AC.X}C_\delta\right) - \Lambda S_\theta S_\delta r_{AC.Z},
\end{aligned}
$$

where

$$H_{11} = J_{\zeta\zeta}.$$

For equation (27):

$$
\begin{aligned}
J_1 &= J_{11}\ddot{\delta} + J_{12}\ddot{y}_A, \\
J_2 &= mS_\delta l_\zeta, \\
J_3 &= -\Lambda C_\theta,
\end{aligned}
$$

where

$$
\begin{aligned}
J_{11} &= -mC_\delta l_\zeta, \\
J_{12} &= m.
\end{aligned}
$$

For equation (28):

$$\begin{aligned} K_1 &= K_{11}\ddot{\delta} + K_{12}\ddot{z}_A, \\ K_2 &= mC_\delta C_\phi l_\zeta, \end{aligned}$$

where

$$\begin{aligned} K_{11} &= mS_\delta C_\phi l_\zeta, \\ K_{12} &= m. \end{aligned}$$

The functions and coefficients of the EOMs given in equations (37)-(38) are:

$$M_1 = J_{11}\ddot{\delta} + M_{11}\ddot{y}_A + M_{12}\ddot{y}, \tag{47}$$

and

$$R_1 = K_{11}\ddot{\delta} + R_{11}\ddot{z}_A + R_{12}\ddot{z}, \tag{48}$$

where

$$\begin{aligned} M_{11} &= J_{12} + \mu, \\ M_{12} &= \mu, \\ R_{11} &= K_{12} + \nu, \\ R_{12} &= \nu. \end{aligned}$$